The biofilm matrix scaffold of *Pseudomonas* species contains non-canonically base paired extracellular DNA and RNA

Thomas Seviour[1,*], Fernaldo Richtia Winnerdy[2], Lan Li Wong[1], Xiangyan Shi[2], Sudarsan Mugunthan[1], Remi Castaing[3], Sunil S Adav[4], Gurjeet Singh Kohli[1], Heather M Shewan[5], Jason R Stokes[5], Scott A. Rice[1,6,7], Anh Tuân Phan[2] and Staffan Kjelleberg[1, 7, 8,*]

[1] Singapore Centre for Environmental Life Sciences Engineering, Nanyang Technological University, 637551, Singapore.

[2] School of Physical and Mathematical Sciences, Nanyang Technological University, 637371, Singapore.

[3] Materials and Chemical Characterisation Facility (MC^2), University of Bath, BA27AY, Bath, United Kingdom.

[4] Singapore Phenome Centre, Nanyang Technological University, 636921, Singapore.

[5] School of Chemical Engineering, The University of Queensland, 4072, Brisbane, Australia.

[6] The iThree Institute, The University of Technology Sydney, Sydney, 2007, Australia.

[7] School of Biological Sciences, Nanyang Technological University, 637551, Singapore.

[8] Centre for Marine Science and Innovation, School of Biological, Earth and Environmental Sciences, University of New South Wales, Sydney, 2052, Australia.

*Correspondence to: twseviour@ntu.edu.sg; laskjelleberg@ntu.edu.sg

Abstract

While extracellular DNA (eDNA) is recognized as a critical biofilm matrix component, it is not understood how it contributes to biofilm function. Here we isolate eDNA from *Pseudomonas* biofilms using ionic liquids, and discover that its key biophysical signatures, i.e. fluid viscoelasticity, nucleic acid conformation, and temperature and pH dependencies of gel to solution transitions, are maintained. Solid-state analysis of isolated eDNA, as a proxy for eDNA structure in biofilms, revealed non-canonical Hoogsteen base pairs, triads or tetrads involving guanine and thymine or uracil. These were less abundant in chromosomal DNA and undetected as eDNA underwent gel-sol transition. Purine-rich RNA was present in the eDNA network, which potentially enables eDNA to be the main cross-linking exopolymer in the matrix through non-canonical nucleobase interactions. Our study suggests that *Pseudomonas* assemble extracellular DNA and RNA into a network with viscoelastic properties, which underpin their persistence and spreading, and may aid the development of more effective controls for biofilm-associated infections.

36 ## Introduction

37 Biofilms are key microbial ecosystems that contribute to bacterial pathogenicity (1), disrupt flow
38 in water filtration systems (2) and facilitate wastewater treatment bioprocesses (3). They
39 represent bacterial adaptation strategies allowing for increased antibiotic tolerance (4), enhanced
40 resource capture (5) and the establishment of ecological microniches (6). Such properties are
41 unique to biofilms, in contrast to planktonic bacteria, and are not mediated directly by the cells
42 but instead by an extracellular polymeric matrix the cells secrete (7). While cells themselves are
43 stiff and rigid, the matrix provides the biofilm with a viscoelastic property that allows cells to
44 withstand mechanical and chemical stress, and enhances surface colonization by facilitating
45 biofilm migration. Moreover, the viscoelastic property of the matrix itself has been identified as
46 a virulence factor in chronic biofilm infections (8).

47 Exopolymer functions in biofilms have been studied extensively, particularly for *Pseudomonas*
48 *aeruginosa*, which contributes to one in five clinical infections (9). No fewer than eight
49 exopolymers have been identified as supporting key traits in *P. aeruginosa* biofilms, including
50 three exopolysaccharides (10), four proteins (11-13) and extracellular DNA (eDNA) (14). While
51 progress has been made towards describing the structures and identities of extracellular
52 polysaccharides and proteins, by applying classical chemical and molecular approaches, the
53 important question regarding extracellular DNA is not what it is but how it differs structurally
54 from chromosomal DNA and what enables it to perform a structural function in the biofilm
55 matrix. eDNA has been described as a key matrix biopolymer in clinical (15) and environmental
56 biofilms (16), particularly in *P. aeruginosa* biofilms (13), and has been shown to colocalize with
57 putative *P. aeruginosa* polysaccharide Pel (17) and be degraded by DNA-specific endonucleases
58 (18). While there have been attempts to explain the properties of eDNA, they have tended to

59 focus on primary-structure differences with the chromosomal DNA and as yet, no signature
60 eDNA sequences have been identified (19).

61 DNA can form multiple higher-order structures arising from differences in torsional stress as the
62 two strands are twisted around the axis. For chromosomal DNA (cDNA), this is known to consist
63 of supercoiled duplex structures that are formed by the action of histone-like proteins and
64 topoisomerases, and then relaxed by gyrases to allow replication and transcription to occur (20).
65 DNA supercoiling, however, does not reconcile with descriptions of eDNA as a primary biofilm
66 structural agent which would imply a networked structure. While eDNA has been shown to
67 colocalize with DNA-binding proteins (21), this does not distinguish it from chromosomal DNA
68 nor allude to its higher-order structure. We propose that a molecular understanding of how the
69 eDNA is assembled and organized is key to answering how and why DNA transforms from the
70 chromosomal form to that found in the biofilm matrix. In this study, we elucidate molecular
71 interactions that lead to the higher-order structure of eDNA. We seek to contrast the biophysical
72 properties of eDNA and chromosomal DNA and correlate differences to a distinct eDNA
73 molecular signature. We hypothesize that isolating eDNA such that its higher-order structure is
74 preserved should enable us to describe interactions in eDNA that underpin its ability to form
75 networked structures.

76 Results

77 eDNA elasticity is preserved during extraction.

78 To isolate eDNA from *P. aeruginosa* biofilms while preserving its higher-order structure, we use
79 ionic liquid 1-ethyl-3-methyl-imidazolium acetate (EMIM-Ac). This has been previously shown
80 to non-destructively dissolve a range of recalcitrant biopolymers, including DNA (22) and

81 cellulose (23), and we recently demonstrated its use in dissolving *P. aeruginosa* biofilm
82 exopolymers (24). Here, we consider the change in fluid rheology upon dissolving *P.*
83 *aeruginosa* biofilms in EMIM-Ac, whereby we observe the subsequent fluid to be highly
84 viscoelastic which is characteristic of high molecular weight polymers in solution. We observe
85 viscoelasticity, in that the EMIM-Ac following biofilm dissolution displayed both elastic and
86 viscous characteristics, upon measuring a normal force during viscosity measurements on a
87 parallel plate rheometer as a function of shear rate under steady shear conditions. The viscosity is
88 only slightly shear-thinning (Supplementary Figure 1A and Supplementary Table 1). Normal
89 force (i.e. contact force perpendicular to the parallel plates applying shear), however, is zero for
90 Newtonian fluids and thus the observation of finite values indicates the presence of an
91 anisotropic polymer in the fluid, giving rise to non-linear elasticity, which is expected for dilute
92 polymer solutions in viscous Newtonian fluids (i.e. Boger fluids) (25). Normal force is
93 characterized as a normal stress difference ($\Delta N = N_1 - N_2$), where N_1 and N_2 are primary and
94 secondary normal stress differences respectively (see definition in Materials and Methods (26)).
95 The fluid's elasticity is observed to dominate over the viscous flow properties for the wild type
96 biofilm in EMIM-Ac, whereby ΔN is an order of magnitude greater than shear stress (Figure 1A;
97 Wild type). The solvent (EMIM-Ac) alone exhibited no elasticity, indicating that the elastic
98 properties arise from the dissolution of polymeric components within the biofilm matrix. ΔN has
99 a power law dependence on the shear rate with an exponent (n) of 1.4 (Supplementary Figure 1B,
100 Wild type). We find that the viscosity and non-linear elasticity measurements are accurately
101 modeled using the modified, finitely-extensible nonlinear elastic (FENE-P) polymer model
102 (Figure 1A-B; Supplementary Tables 1 and 2), which is commonly used to describe solutions
103 containing flexible/semi-flexible polymers using the common assumption that $\Delta N \sim N_1$ (27). As

104 DNA is a very high molecular weight semi-flexible polymer, we hypothesize that this may be the
105 dominant polymer giving rise to the nonlinear elastic properties of the fluids.

106 The polysaccharides alginate, Pel and Psl have been suggested as the structural scaffolds of *P.*
107 *aeruginosa* biofilms (10). To investigate the possibility that the polysaccharides, rather than the
108 DNA, cause the elastic behavior of the fluid after biofilm dissolution, an alginate over-
109 expressing strain PDO300 (i.e. mucoid) and its isogenic Pel and Psl genetic knockout mutants
110 were dissolved in EMIM-Ac (28). When Psl is absent, the elasticity (i.e. ΔN) and viscosity
111 increase relative to the wild type, and the mucoid strain PDO300 is less elastic than the wild type
112 despite the over-expression of alginate (Figure 1; Δ*psl*). In contrast, when Pel is absent, there
113 was a slight decrease in both elasticity and viscosity relative to both the wild type and PDO300
114 (Figure 1; Δ*pel*).

115 The contributions of proteins, RNA and DNA were also explored by digestion using pronase,
116 RNase A and DNase I, respectively (Figure 1; Pronase, RNase, DNase). Removing each
117 exopolymer component individually decreased biofilm elasticity in EMIM-Ac. All treatments,
118 except for DNase I-treated biofilm, displayed n values of 0.9 – 1.7 (Supplementary Table 1),
119 characteristic of elasticity imparted by DNA (29). While viscosity was unchanged following
120 pronase treatment, there was a slight decrease in elasticity. This decrease in elasticity was even
121 greater following RNase treatment and elasticity was completely lost upon DNase treatment,
122 with ΔN reduced to zero. We suggest that the elastic response of the biofilm in EMIM-Ac can
123 thus be primarily attributed to DNA. Elasticity was not detected in EMIM-Ac solutions of calf
124 thymus DNA at the same concentration, indicating that elasticity is not a universal property of
125 DNA solutions in EMIM-Ac.

126 Furthermore, characterization of linear viscoelastic properties of hydrated native *P. aeruginosa*
127 biofilms (i.e. in water rather than EMIM-Ac) under conditions of oscillating shear show that the
128 storage (or elastic) modulus (G') is greater than the loss (or viscous) modulus (G'') across the
129 frequency range 0.1 to 1 s^{-1}, even in the absence of Pel and Psl (Figure 1C), providing further
130 evidence that they are not primarily responsible for the viscoelastic property of the biofilm. This
131 is consistent with the hydrated biofilm being classified as a gel. A storage modulus could not be
132 measured following digestion of the native biofilm by DNase I, and biofilm digested with heat-
133 inactivated DNase I also remained as a gel, illustrating that the lack of measurable G' was due to
134 enzymatic activity (Supplementary Figure 1C).

135 DNA is thus considered the main contributor to the elastic gel-like rheology of *P. aeruginosa*
136 biofilms, and to the non-linear elasticity upon dissolution of lyophilized *P. aeruginosa* biofilm in
137 EMIM-Ac. The fundamental structure of the DNA within the two systems is different; a gel-like
138 rheology may arise from a polymer network structure, while the non-linear elasticity indicates
139 the movement and deformation of high molecular weight polymers during flow. The approach of
140 dissolving biofilm in EMIM-Ac therefore allows the assessment of the contribution of individual
141 exopolymers to its properties that is complemented by rheological assays on the native biofilms.

142 The data suggest that multiple exopolymers contribute to the rheology, with the matrix from the
143 Δ*psl* mutant being the most elastic, followed by wild type and RNase A-treated biofilms, which
144 were the least elastic. It has been noted previously that a range of *P. aeruginosa* exopolymers
145 influence biofilm extracellular matrix crosslinking (10) and the data presented here further
146 clarify that these exopolymers can only modulate biofilm rheology if eDNA is present. An
147 eDNA scaffold is therefore a prerequisite for this rheological differentiation of the matrix.
148 Further support for the presence of an eDNA scaffold is provided in the micrograph of a biofilm

149 stained with TOTO-1 for DNA visualization (Figure 1D), which shows DNA fibers in the

150 extracellular matrix.

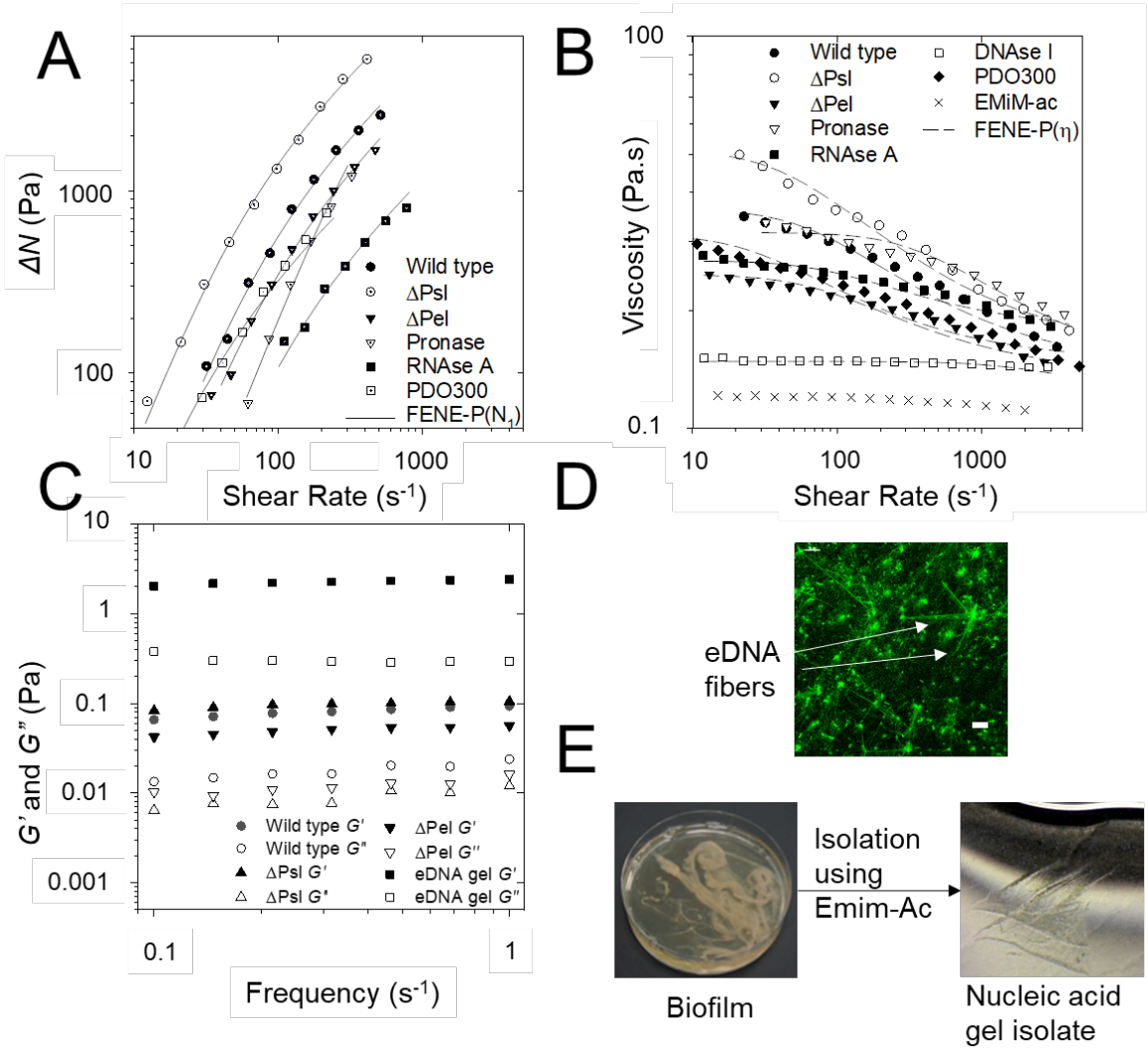

151

152 **Figure 1:** (A) Non-linear elasticity as normal stress difference ($\Delta N = N_1 - N_2$) and (B) viscosity against shear rate for

153 *Pseudomonas aeruginosa* biofilm wild type, PDO300, Δ*psl*, Δ*pel*, and pronase, RNase A and DNase I digested wild

154 type biofilm in 1-ethyl-3-methylimidazolium acetate (40 mg/mL) at 25 °C, 250 µm gap. This is measured as a

155 function of shear stress from 10 to 1000 Pa. ΔN is not described for DNase I digested biofilm in Figure 1A and

156 Supplementary Figure 1B as their normal force (F_N) is less than the resolution of the rheometer (i.e. 0.1 N) and set to

157 zero for calculating ΔN. Both the ΔN and viscosity data are fitted with the FENE-P model, a rigid dumbell model for

158 polymer solutions. Fitting parameters are shown in Supplementary Table 2. (C) Frequency dependence rheogram

159 showing that storage (G' or elastic) exceeds loss (G'' or viscous) modulus for wild type, Δ*psl* and Δ*pel* biofilms and
160 isolated eDNA gel at 25°C (250 µm plate gap). (D) Micrograph of *P. aeruginosa* biofilm DNA stained green with
161 TOTO-1 (scale bar 10 µm). (E) Phase separation of extracellular DNA extracted from *P. aeruginosa* biofilms into a
162 gel occurs upon transfer from 1-ethyl-3-methylimidazolium acetate (EMIM-Ac) into water.

163 The absence of phospholipids and lipopolysaccharides in EMIM-Ac following biofilm
164 dissolution demonstrate that EMIM-Ac did not lyse either biofilm or planktonic cells
165 (Supplementary Figure 2A). Therefore, it was concluded that the DNA dissolved following
166 treatment of *P. aeruginosa* biofilms with EMIM-Ac is extracellular and not due to extraction of
167 intracellular DNA.

168 **Key biophysical signatures of nucleic acids are preserved during isolation.**

169 We recovered the eDNA from EMIM-Ac following biofilm dissolution by exploiting the ability
170 of perchloric acid to selectively precipitate DNA over protein (Supplementary Figure 2B).
171 Following further purification by gel permeation chromatography, the polymer phase-separated
172 into a gel upon transfer from EMIM-Ac into water (i.e. the gel isolate), mimicking the formation
173 of networks in native biofilms (Figure 1E). G' exceeded G'' across the same frequency range as
174 for the hydrated, native *P. aeruginosa* biofilms, consistent with gels, as was the case for the
175 biofilms (Figure 1C) and as distinct from the viscous behavior (G' < G'') commonly displayed
176 by aqueous solutions of DNA (30). Furthermore, DNase degraded the isolated gel into shorter
177 DNA fragments (Supplementary Figure 3A). Other fractions, including those not precipitated by
178 perchloric acid, did not self-assemble into gels (Supplementary Figure 3B). Similarly, calf
179 thymus DNA did not form gels when processed the same way, either with or without added
180 cations (Supplementary Figure 3C) suggesting, once again, that networking and elastic behavior
181 is not a general feature of DNA under the conditions applied in this study. Moreover, the biofilm

182 and isolated eDNA displayed similar phase transition temperatures of 56.8 and 57.2°C,
183 respectively (Supplementary Figures 4A and 4B), and the elasticity described for the isolated
184 eDNA and biofilm in Figure 1C was lost at temperatures exceeding the phase transition
185 temperatures and upon alkalinization (i.e. 0.2 M NaOH).

186 Circular dichroism (CD) is a highly sensitive spectroscopic technique for determining the
187 secondary structure of biomolecules, particularly proteins and nucleic acids. It was used here to
188 understand whether the nucleic acid (NA) conformation was modified during extraction and
189 isolation. Unprocessed *P. aeruginosa* biofilms displayed a major circular dichroism (CD) peak at
190 250-285 nm (Figure 2A), which is consistent with the presence of NA (31) and this peak was
191 also observed to dominate the CD spectrum of the gel isolate (Figure 2B). The spectral trough at
192 225.5-226.5 nm is typical for proteins (32). NA can also display a trough in this region, although
193 the relative depth of the trough and its absence after proteolysis and fractional precipitation that
194 excludes proteins (Supplementary Figure 2B) suggest that it denotes proteinaceous material.
195 Nonetheless, while the CD spectrum shows that proteins are significant components of the
196 biofilm matrix, as indicated by Figure 1A they are not major contributors to biofilm elasticity.

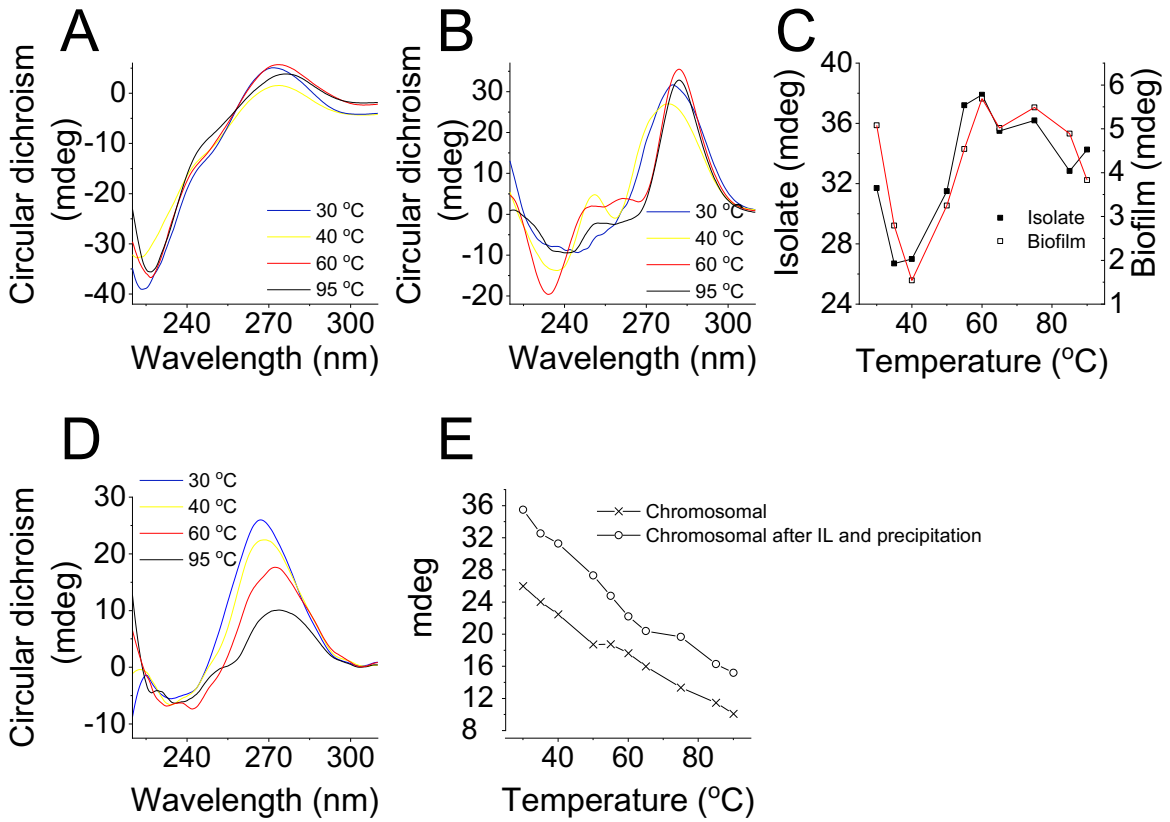

Figure 2: Representative circular dichroism (CD) spectra of (A) *Pseudomonas aeruginosa* biofilm and (B) eDNA gel isolate at 30°C (blue), 40°C (yellow), 60°C (red) and 95°C (black) dialysed against double distilled water. (C) Amplitude of dominant NA peak, CD_{max} (260-285 nm), from CD spectra of *P. aeruginosa* biofilm (seen in (A)) and its extracted extracellular nucleic acid gel (i.e. isolate) (seen in (B)) from T = 30°C to T = 95°C. (D) Representative CD spectra of *Pseudomonas aeruginosa* biofilm chromosomal DNA in double distilled water at 30°C (blue), 40°C (yellow), 60°C (red) and 95°C (black). (E) Amplitude of dominant NA peak, CD_{max} (260-285 nm), from CD spectra of *P. aeruginosa* biofilm chromosomal DNA (seen in (D)) from T = 30°C to T = 95°C with and without solubilization in 1-ethyl-3-methylimidazolium and fractional precipitation.

The CD spectrum of the isolated eDNA gel (Figure 2B) is dominated by the same NA peak that appears in the biofilm CD spectrum. CD melting experiments were then performed on both samples. The resulting melting curves (Figure 2C) show that their NA peak absorbance values follow the same trend across the temperature profiles with a maximum at their phase transition, or melting temperatures (i.e. T_m) of (i.e. ≈ 57°C), indicating that melting occurs due to an eDNA

211 gel-sol transition and that heating disrupts the higher order structure of NA. In contrast, the NA
212 peak in chromosomal DNA extracted from *P. aeruginosa* planktonic cells decayed steadily with
213 temperature (Figure 2D and 2E). This was also observed for chromosomal DNA processed
214 through ionic liquid (i.e. EMIM-Ac dissolution and fractional precipitation).

215 Thus, *P. aeruginosa* eDNA has a different higher order structure to its chromosomal DNA. The
216 elastic behavior observed throughout purification and faithfully preserved in the isolated eDNA,
217 is not a consequence of the processing method. The extracted eDNA gel isolate is therefore an
218 accurate proxy for understanding the intermolecular interactions that stabilize the extracellular
219 matrices of *P. aeruginosa* biofilms. Moreover, the CD spectrum of the eDNA gel (Figure 2B)
220 indicates multiple nucleic acid conformations. In addition to the peak at 272 nm, there is a trough
221 that shifts from 245 to 230 nm with increasing temperature, another maximum at 215 nm that
222 remains constant with temperature, and other sub-maxima at 260 and 253 nm that change with
223 temperature. The absence of a trough at 200-215 nm precludes the possibility of NA in A- or Z-
224 conformations (31). The dominant maximum and minimum could indicate either B-DNA or G-
225 quadruplex conformations (33), although the peak at 215 nm is not a feature of B-DNA CD
226 spectra and is slightly higher than the characteristic G-quadruplex low wavelength peak of 210
227 nm. Nonetheless, the appearance of several peaks in the NA region of 250-285 nm indicates that,
228 while the dominant NA conformation is unclear, several conformations likely contribute to phase
229 separation of the NA.

230 **Non-canonical base pairs or tetrads support extracellular network.**

231 Sequence analysis of the extracted material indicated that the gene coverage was even for both
232 chromosomal and eDNA with the exception of bacteriophage Pf4 genes (Supplementary Figure
233 5). However, the Pf4 knockout mutant of *P. aeruginosa* also displayed an elastic response when

234 dissolved in EMIM-Ac (Supplementary Figure 6, Supplementary Tables 1 and 2), indicating that
235 Pf4 DNA is unlikely to be responsible for the phase-separating behavior of *P. aeruginosa*
236 biofilms. The biophysical properties of eDNA cannot be explained by uneven gene coverage,
237 including the expression of Pf4.

238 To describe the nature of nucleic acid base-pair interactions contributing to the elastic behavior
239 of the isolated eDNA we performed Magic-angle spinning (MAS) solid-state NMR (SSNMR).
240 This technique is ideal for intractable systems such as biofilms to eliminate solubility and
241 extraction biases (34), and to analyze inter-molecular H-bond interactions to describe, for
242 instance, inter-nucleotide base pairing in RNA (35). MAS SSNMR averages anisotropic
243 interactions to provide high-resolution spectral characterization of insoluble and large
244 biomolecular systems. By analyzing dipolar interactions, through-space heteronuclear
245 correlations (e.g. N···H) can be detected.

246 To elucidate the mechanism of DNA gelation, we generated, by SSNMR, a 2D, through-space,
247 ^{15}N-^{1}H HETCOR spectrum of ^{15}N labeled eDNA gel isolated from *P. aeruginosa* biofilm matrix.
248 The absence of signature protein and polysaccharide peaks in the ^{15}N-^{1}H HETCOR spectrum
249 confirmed the complete absence of proteins and polysaccharides in the gel isolate
250 (Supplementary Figure 7), which supports our assertions that neither contribute to eDNA
251 gelation, despite the fact that both have been reported previously to co-localize with eDNA
252 (17,21). The HETCOR spectrum across the imino proton region showed four signal clusters at δ_H
253 10-14 ppm, and δ_N 140-160 ppm (Figure 3), which arose from direct N-H couplings of T/U and
254 G nucleobase imino groups. Two of these clusters (δ_H 12-14 ppm) resulted from imino protons
255 hydrogen-bonded to a nucleobase nitrogen (i.e. N-H···N), and the other two (δ_H 10 -12 ppm)
256 from imino protons hydrogen-bonded to a nucleobase carbonyl oxygen (i.e. N-H···O) (36). Due

to the longer cross polarization times we were able to observe a strong, long-range and indirect (i.e. intermolecular) correlation at δ_N 196 ppm arising from G-C Watson-Crick base pairing, i.e. C(N3)-G(H1). There was also a weak and indirect correlation at δ_N 220 ppm resulting from A-T/U Watson-Crick base pairing, i.e. A(N1) to U/T(H1).

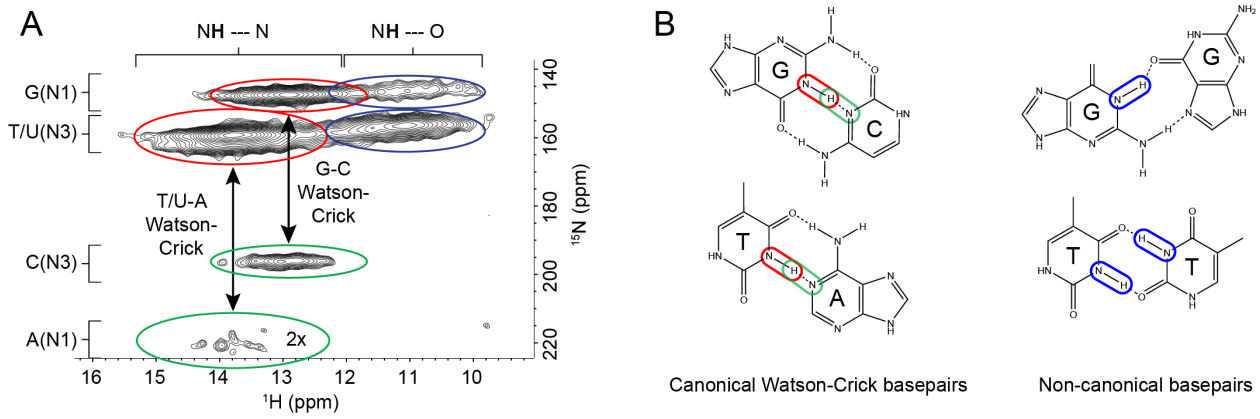

Figure 3: (A) Representative solid-state 2D ^{1}H-^{15}N through-space heteronuclear correlation (HETCOR) spectrum of extracellular nucleic acid (NA) gel isolate dialysed against double distilled water (2 mg), T = 25°C. Red ovals show the cross-peaks from direct N-H couplings of G (N1-H1) and T/U (N3-H3) when the protons were hydrogen bonded to nucleobase nitrogen atoms (i.e. NH···N). Green ovals present the cross-peaks generated form indirect (via hydrogen bonds) N-H couplings between the G(H1) and C(N3) as well as between T/U(H3) and A(N1). The threshold for the A(N1)-T/U(H3) correlation was increased due to lower signal intensity for that particular coupling. Cross-peaks denoted by red and green ovals indicate Watson-Crick G-C and U/T-A base pairings respectively. Blue ovals show cross-peaks from direct N-H couplings of G (N1-H1) and T/U (N3-H3) when the protons were hydrogen bonded to carbonyl oxygen (i.e. NH···O). These cross-peaks reveal non-canonical base pairings between G, T or U and G, T, U or C as well as the possibility of G-tetrad formations. (B) Canonical and non-canonical base pairing schematics illustrate the possible H-bond interactions between imino protons of A and G that can be observed in the HETCOR spectrum. The correlations are color-coded to match the spectrum. Covalent and hydrogen bonds are indicated by solid and dashed lines respectively.

277 The observation of NH to O interactions suggests the occurrence of non-canonical base pairs,
278 triads or tetrads involving G and T/U. The absence of long-range correlations between the
279 clusters at δ_H 10 -12 ppm is also consistent with non-Watson-Crick pairings for the G and T/U
280 nucleobases, where Hoogsteen H-bonded G-bases can assemble planarly into tetrads and self-
281 stack to form structurally stable G-quadruplexes (37). δ_H assignments of imino protons H-bonded
282 to nucleobase carbonyl O and N respectively are validated by 1-D ^{1}H NMR spectra of well-
283 characterized G-quadruplex and canonical B-DNA structures (Supplementary Figure 8A and
284 8B), and of a DNA quadruplex-duplex structural hybrid (Supplementary Figure 8C).

285 To determine whether non-canonical base pairs contribute to eDNA elasticity, a ^{15}N-^{1}H
286 HETCOR spectrum was recorded for ^{15}N labeled-eDNA gel after heating it to above the gel-sol
287 transition temperature. In contrast to the sample without heating (Figure 4A), no non-canonical
288 base-pair ^{15}N-^{1}H interactions were detected in the sample heated to 65°C (Figure 4B). The
289 Watson-Crick base-pair interactions, on the other hand, persisted with and without heating.
290 Similarly, the chromosomal DNA of *P. aeruginosa*, which does not exhibit the elastic or gel-like
291 behavior characteristic of the eDNA (Figure 2D and 2E), displayed no NH to O interactions,
292 which is consistent with the absence of non-canonical base-pair interactions (Figure 4C). Only
293 canonical base-pair interactions were observed in the ^{15}N-^{1}H HETCOR solid state spectrum of P.
294 aeruginosa PAO1 chromosomal DNA before (green) and after (gold) receiving the same
295 treatment as eDNA, demonstrating that non-canonical base pair interactions are specific for the
296 eDNA of *P. aeruginosa* and not an artifact of extraction and processing. Hence, the non-
297 canonical base pairs, triads or tetrads are characteristic of eDNA in a gel or networked state and
298 may contribute to stabilizing the higher order structure of eDNA networks.

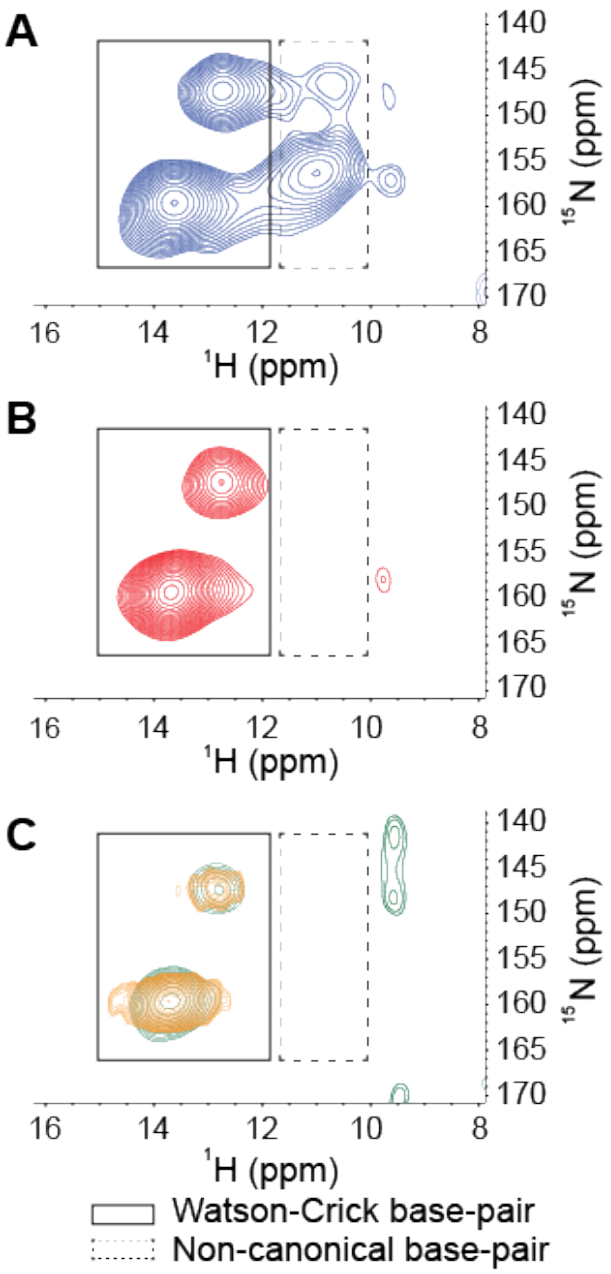

299

300 **Figure 4:** Representative solid-state 2D ^{1}H-^{15}N through-space heteronuclear correlation (HETCOR) spectrum of

301 ^{15}N-labelled extracellular nucleic acid (NA) gel isolate in double distilled water (2 mg), including direct N-H

302 coupling region only, at T = 25°C with no pre-heating (A) and with pre-heating to 65°C (B), and ^{15}N-labelled

303 chromosomal DNA extracted from *Pseudomonas aeruginosa* biofilms in double distilled water before (green) and

304 after (gold) receiving the same treatment as the extracellular nucleic acids (C), indicating the loss of non-canonical

305 base pairings, triads or tetrads in the gel isolate upon heating and their absence in chromosomal DNA.

306 **Purine-rich RNA is also a component of eDNA gel.**

307 Total correlation spectroscopy (TOCSY) and ^{1}H-^{13}C heteronuclear single quantum coherence
308 (HSQC) are nuclear magnetic resonance (NMR) techniques that can identify proton NMR
309 correlations within individual ribose sugars and their proton-carbon single bond correlations
310 respectively. Raising the pH can solubilize *P. aeruginosa* biofilms (38) and here we show that
311 after alkalinization, the NA peaks dominate the solution ^{1}H-^{13}C HSQC spectra for the isolated
312 material which provides further evidence that proteins or polysaccharides were absent
313 (Supplementary Figure 9A) (39). However, the ^{1}H-^{13}C HSQC-TOCSY spectrum of the isolated
314 gel when dissolved by alkalinization showed two clusters of sugar proton peaks (C1'-H1') with
315 correlations to neighboring carbons (C2'-H1') (Figure 5A). This demonstrates that there are two
316 types of nucleic acid present and contributing to the composition of the isolated gel.

317 The first cluster (rectangles) has C2' chemical shift values of ~40 ppm and the second cluster
318 (ovals) has C2' values of ~70 ppm. The ^{1}H-^{13}C correlations denoted by the rectangles therefore
319 arise from deoxyribose and those denoted by the ovals from ribose sugar conformations. The
320 broadened form of the deoxyribonucleotide peaks is consistent with high molecular weight
321 (MW) molecules, while the sharpness of the ribonucleotide peaks suggests that they arise from
322 small nucleotides. Hence, eDNA and small ribonucleotides are both likely to be present in the
323 gel dissolved by alkalinization.

324 Spin-systems (i.e. groupings of nuclei that do not couple with nuclei beyond their respective
325 systems) for the eight sharp ribonucleotide peaks (Figure 5B) were assigned by HSQC-TOCSY
326 and correlation spectroscopy (COSY) (Supplementary Figure 9B) with absolute identification
327 achieved by heteronuclear multiple bond correlation spectroscopy (Supplementary Figure 10).
328 The ^{31}P NMR spectrum of the eDNA gel isolate at elevated pH revealed the presence of a
329 mixture of monoesterified (3.4 to 4.1 ppm) and diesterified phosphates (-0.8 to -1.2 ppm),

330 indicating the coexistence of monoribonucleotides and DNA respectively (Figure 5C (i)). Long-
331 range ^{31}P-^{1}H correlations (i.e. from NA phosphorous to adjoined ribose proton) were observed in
332 the ^{31}P-^{1}H heteronuclear correlation (HETCOR) spectrum (Figure 5C (ii)) for both
333 monoribonucleotides and DNA. The broad ^{31}P-^{1}H cross peaks at ~-1.0 ppm (Figure 5C (ii))
334 correspond to long-range correlations between DNA phosphorous to H3' and H5'/H5'' protons.
335 The eight monoribonucleotides were assigned to 2'- and 3'-(A, U, G, and C)-monophosphates.
336 We therefore have both 2' and 3' monoribonucleotides present with the eDNA in the gel
337 solubilized under alkaline conditions.

338 Importantly, the monoribonucleotide peaks only became resolved upon alkaline dissolution of
339 the biofilm, in contrast to the broad peaks evident at pH 7 (Supplementary Figure 11A). This
340 indicates that the monoribonucleotides are derived from chain structures that exist at biological
341 pH, which is consistent with the observation in Figure 1A that RNA is a major contributor to *P.*
342 *aeruginosa* biofilm elasticity.

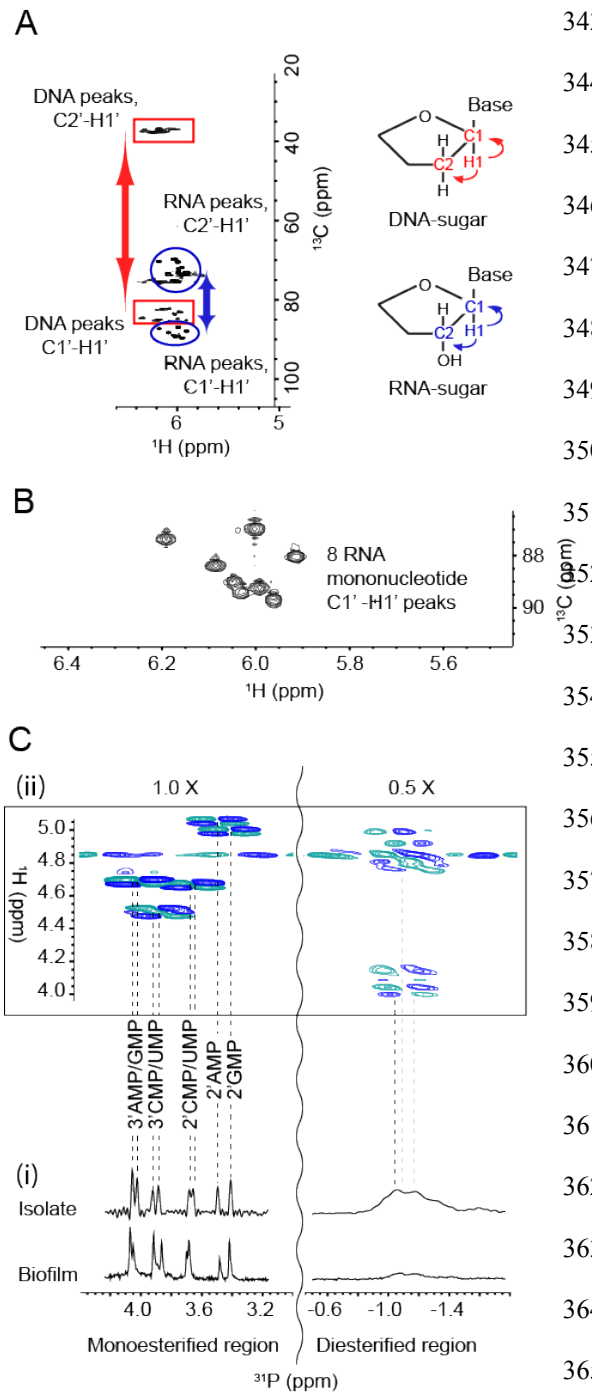

Figure 5: (A) Representative Nuclear magnetic resonance (NMR) ^{1}H-^{13}C heteronuclear single quantum coherence (HSQC)-total correlation spectroscopy (TOCSY) spectrum at 25°C of extracellular nucleic acids (NA) gel isolate after alkalinization showing the C1'-H1' cross peaks of RNA (blue ovals) and DNA (red rectangles) and their correlations to the neighboring carbon C2'-H1'. Schematics (right) illustrate these correlations. (B) ^{1}H-^{13}C HSQC spectrum of extracellular eDNA gel isolate at 25°C after alkalinization identifying eight monoribonucleic acid ribose spin systems. (C) 1-D ^{31}P NMR of NA isolate gel and *Pseudomomonas aeruginosa* biofilm with proton decoupling showing the presence of monoesterified (i.e. monoribonucleotides) and diesterified (i.e. DNA) phosphate peaks (i), and 2-D ^{1}H-^{31}P heteronuclear correlation (HETCOR) spectrum of extracellular NA showing the ^{31}P-^{1}H cross-peaks of monoribonucleotides and DNA (ii). Couplings of monoesterified phosphates to H2' or H3' of eight monoesterified monoribonucleotides (from left to right: 3' AMP/3' GMP, 3' CMP/3' UMP, 2' CMP/2' UMP, 2' AMP, 2' GMP); and diesterified phosphate to DNA H3' and H5'/H5'' protons, are denoted by the dashed lines. There is a discontinuity (wavy line) in the ^{31}P axis due to the different thresholds required to illustrate the ^{31}P-^{1}H correlations in the mono-esterified and di-esterified regions. All samples were prepared in 0.1 M NaOD (10 mg/mL) and preheated to 55°C for 2 h.

The molar ratio of the individual ribonucleotides could be determined from the ^{31}P spectrum of the gel dissolved at high pH (Table 1). While several peaks could not be separated, it was

371 possible to deduce that the RNA is purine rich (i.e. 57 mol% A+G) and that the G+C mol%
372 content of 46-50% differs from that of the *P. aeruginosa* genome (i.e. 67 mol%) (40).
373 Quantification was undertaken on the basis of relative ^{31}P NMR peak areas for the eight
374 monoribonucleotides and is therefore unaffected by the presence of any free nucleic acid bases.
375 The same peaks were also observed in the biofilm ^{31}P spectrum after alkalinization (Figure
376 5C(i)). Sequence analysis of the eDNA (Supplementary Figure 5) indicated that, on the other
377 hand, eDNA nucleobase ratios were consistent with the genome and the presence of canonical
378 nucleotides.

379 **Table 1:** Relative abundances of monoribonucleotides in extracellular eDNA gel isolate from *Pseudomonas*
380 *aeruginosa* biofilm as determined by integrating ^{31}P NMR spectrum following alkalinization.

^{31}P shift (ppm)	Ribonucleotide	Relative abundance
4.03	3'AMP	18 %
4.01	3' GMP	17 %
3.90	3' CMP/3' UMP	9 %
3.87	3' CMP/3' UMP	11 %
3.68	2' CMP/2' UMP	10 %
3.66	2' CMP/2' UMP	12 %
3.50	2' AMP	10 %
3.42	2' GMP	13 %

381

382 In contrast to the liquid state ^{31}P NMR spectrum of the alkali-dissolved isolate (Figure 5C (i)),
383 the ^{31}P SSNMR spectrum of the gel isolate (i.e. no alkali treatment; Figure 6A (i)) showed a
384 single peak in the diesterified phosphate region, consistent with the presence of both DNA and
385 RNA chains. There are no sharp peaks present in the monoesterified phosphate region, further
386 demonstrating that the monoribonucleotides are a consequence of alkali transesterification (41).

387 Only the diesterified phosphate peak was observed in the ^{31}P SSNMR spectrum of the biofilm
388 (Figure 6A (iii)), while both RNA-derived monoesterified and DNA-derived diesterified
389 phosphate peaks were present in the ^{31}P SSNMR spectrum of alkali digested eDNA gel-isolate

390 and biofilm (lyophilized) (Figure 6A (ii) and Figure 6A (iv), respectively). Complete alkali RNA
391 transesterification was confirmed by the full conversion of diesterified to monoesterified
392 phosphates (from liquid state ^{31}P NMR spectra) for the RNA standard, when dissolved in 0.1 M
393 NaOH (Supplementary Figure 11B). Conversely, RNA diesterified phosphate peaks were
394 preserved in the RNA standard spectrum following dissolution in EMIM-Ac and recovery by
395 perchloric acid (Supplementary Figure 11C). Hence, the alkaline conditions break down the
396 RNA chains into individual monoribonucleotides, while the ionic liquid-based extraction does
397 not. This suggests that the conventional method for *P. aeruginosa* biofilm dissolution in alkali
398 (38) may in fact work by transesterifying RNA as a primary structural component and illustrates
399 the importance of the ionic liquid-based extraction protocol described here as a non-destructive
400 method for interrogating biofilm structural polymers.

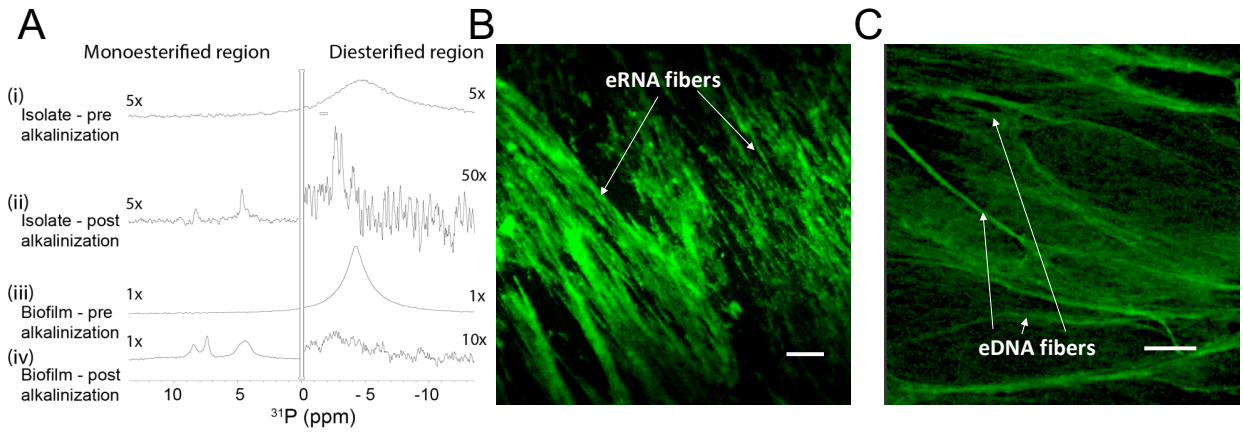

401

402 **Figure 6:** (A) Solid-state ^{31}P NMR spectra at T = 25°C of extracellular eDNA gel isolate (i), alkalinized and
403 lyophilized eDNA gel isolate (ii), *Pseudomonas aeruginosa* biofilm (iii) and alkalinized and lyophilized *P.*
404 *aeruginosa* biofilm (iv) showing the presence of diesterified phosphate peaks and the absence of monoesterified
405 phosphate peaks for both eDNA gel isolate and biofilm in double distilled water, and the coexistence of diesterified
406 and monoesterified phosphate peaks for both samples after alkalinization. This indicates that alkalinization of the

407 matrix results in RNA transesterification. Micrographs of *P. aeruginosa* eDNA gel isolate stained green with (B)
408 SYTO RNASelect showing RNA fibers and (C) TOTO-1 showing DNA fibers (scale bar 10 μm).

409 To visualize the DNA-RNA network organization, we used nucleic acid-specific stains, i.e. RNA
410 specific SYTO RNASelect dye (Figure 6B) and the eDNA-specific TOTO-1 dye (Figure 6C)
411 (42). Fibrous structures, which are typical of networked polymer gels (43), were observed in the
412 eDNA gel isolate stained with both nucleic acid dyes as well as in the biofilm stained with the
413 eDNA specific dye (Figure 1D). This is consistent with our observation that the biofilm is readily
414 degraded by DNase I (Figure 1A) (44). Furthermore, the eDNA gel isolate was stained positively
415 with the RNA-specific dye even after DNase I digestion, providing further evidence that RNA
416 contributes to networking (Supplementary Figure 12A). However, digestion with RNases III, A
417 and H, did not degrade the biofilm (Figure 1A; Supplementary Figure 12B). This may suggest
418 that the RNase binding was shielded by hairpins in the network, or the presence of non-canonical
419 DNA-RNA interactions (45,46). Additionally, while eDNA gel isolate treated directly with
420 RNAse A was not reduced in size (i.e. 1000–4000 nucleotides; Supplementary Figure 12C, Lane
421 D1), gel isolate pre-digested with DNase I (Lane E1) and subsequently digested by RNase A
422 (F1), was degraded from 350-1000 nucleotides into a single band of approximately 150
423 nucleotides. This provides further evidence that extracellular RNA, of MW 350 to 1000
424 nucleotides, are protected from RNase A digestion because they are likely complexed to eDNA.
425 The ScreenTape analysis also shows the absence of clear 23S and 16S RNA bands, unlike the
426 control (Lane G1), indicating that extracellular RNA are either partially degraded or not
427 ribosomal RNA, and highlighting the challenges in detecting and analyzing RNA in the
428 extracellular matrix.

429 The presence of purine-rich RNA was confirmed by LCMS analysis, where the eDNA gel was
430 found to consist of about 4 % w/w RNA although the actual amount is likely to be higher due to
431 incomplete transesterification. Nonetheless, the structural importance of RNA is illustrated by
432 the irreversible pH dependent gel-sol transition displayed by the biofilm (Figure 1C), which
433 occurs coincident with transesterification of RNA and not DNA (Figure 5). If the role of RNA is
434 to facilitate cross-linking of DNA, relatively low amounts of RNA would be required to facilitate
435 its cross-linking.

436 Discussion

437 We extracted a gel-forming complex composed of DNA and RNA from the extracellular matrix
438 of *P. aeruginosa* biofilms without disrupting its fundamental structural or chemical organization.
439 Long-term stability has been reported for various biomolecules in ionic liquids, including DNA
440 (47), and its use here for assessing higher-order eDNA structure is informative. We report the
441 novel observation that extracellular RNA contributes structurally to biofilms and that it
442 contributes along with eDNA to the fundamental viscoelasticity of *Pseudomonas* biofilms. A
443 viscoelastic matrix differentiates planktonic cells from biofilms and the viscoelastic property of
444 the matrix itself is considered a virulence factor in chronic biofilm infections (8). Our data
445 suggest that in forming biofilms *Pseudomonas* assemble their RNA and DNA into an
446 extracellular framework that supports viscoelasticity. Understanding how the DNA and RNA is
447 organized extracellularly during different development stages and in response to environmental
448 conditions is thus central to understanding *Pseudomonas* biofilms.

449 While gel-forming exopolymers have been detected in other biofilms (48), no functional DNA
450 gel has been described for any biological system, much less one also including extracellular
451 RNA. DNA hydrogels are attractive biomaterials due to their biocompatibility, however DNA

452 gelation typically requires either ligase-mediated reactions to induce branched DNA molecule
453 formation (i.e. Y-scaffold), chemical crosslinking agents (e.g. epoxides), cationic
454 poly(electrolytes) (e.g. spermidine) to promote complexes by electrostatic interactions, or
455 physical entanglements (49). The presence of RNA with eDNA therefore addresses the question
456 of how DNA, otherwise favoring linear or circular structures, can form networked structures in
457 biofilms in the absence of, for example, cationic polyelectrolytes. RNA is more structurally
458 versatile than DNA (e.g. hairpins), has a greater tendency to form non-canonical base pairs, and
459 has been shown to undergo a sol-gel transition due to multivalent interactions between strands
460 (50). It informs on why *Pseudomonas* biofilms are readily dissolved by alkalinization, resulting
461 from RNA transesterification, providing further evidence of the structural role of RNA. It also
462 suggests RNA as potential targets for biofilm control, and there are several possible explanations
463 for why RNA nucleobase ratios might deviate from genomic abundances (i.e. 67% G-C for *P.*
464 *aeruginosa*) (51), including small-RNA, microRNA, non-coding RNA, virus RNA and
465 alternative polyadenylation (52).

466 While it is not possible to identify the precise nature of the DNA-RNA interaction based on the
467 information presented in this study, purine-rich RNA as described here for the extracellular
468 eDNA gel isolate (57 mol% A-G) is a characteristic of DNA-RNA duplexes because RNA
469 purines bind more strongly to their DNA pyrimidine complement than vice versa (53). Both
470 Watson-Crick and non-canonical interactions were present in the eDNA gel isolate, which is also
471 consistent with the discrepancy observed between RNA and DNA G+C mol% contents (Table
472 1). It is possible, therefore, that interactions between DNA and RNA, as described in this study,
473 account for the formation of a highly stable nucleic acid gel.

474 The results presented provide unprecedented resolution of the biofilm exopolymeric matrix and
475 its key foundation structural components. We have developed a methodology that preserved the
476 molecular organization of the foundational polymer in its native state upon extraction and
477 isolation. This enabled us to use SSNMR to describe intermolecular associations at the atomic
478 level.

479 This study demonstrates that an eDNA-RNA network, responsible for the elastic gel-like
480 properties of the matrix, contributes greatly to the formation of a physically distinct habitat in the
481 matrix of *P. aeruginosa* biofilms, which in turn is responsible for emergent properties such as
482 nutrient accumulation, stress and antibiotic resistance, and shelter (54). This finding is a
483 departure from the prevailing paradigm that biofilm gelation is only due to polysaccharides. The
484 elastic and biofilm-forming properties were also observed for *Pseudomonas putida* and
485 *Pseudomonas protegens* (Supplementary Figures 6 and 13; Supplementary Tables 1 and 2)
486 suggesting that eDNA is broadly important for biofilm formation in member species of this
487 genus. In addition to *Pseudomonas* spp., other organisms are known to have eDNA, including
488 the clinically relevant organisms *Staphylococcus aureus* (55), *Staphylococcus epidermidis* (56)
489 and *Mycobacterium abscessus* (57) as well as environmental isolates such as strain F8 from the
490 South Saskatchewan River (16).

491 While eDNA is commonly thought to be the product of cell lysis, and has been shown to be
492 released by a sub-population of lytic *P. aeruginosa* cells (19), there is an increasing awareness
493 that it serves an important structural function, such as in activated sludge granules (58).
494 Additionally, Bockelmann et al.(16) observed that stable filamentous networks produced by the
495 aquatic strain F8 were comprised of DNA. The present study provides the first account of a
496 structural signature for eDNA, absent in the chromosomal DNA. However, the environmental

497 factors contributing to eDNA release and how this is regulated (i.e. whether it is an active or
498 passive process) are still unclear. It is possible that DNA-RNA foundational gel networks, as
499 described here for the Pseudomonads, are broad-scoping phenomena in biofilms, and that
500 interactions with RNA enable an extracellular structural function for DNA more broadly. Thus,
501 elucidating how nucleic acids, including RNA, are integral to the biophysical and other emergent
502 properties imparted on the biofilm via the extracellular matrix, will inform the regulation and
503 control of extracellular nucleic acid release across environmental and clinical biofilms.

504 Materials and Methods

505 Bacterial strains

506 Unless otherwise stated, all experiments were undertaken directly on *P. aeruginosa* PAO1
507 biofilms grown in lysogeny broth (LB) at 37°C. The *P. aeruginosa* PAO1 Δ*pf4* knockout mutant
508 is a defined Pf4 chromosomal deletion mutant of the entire Pf4 prophage genome (59). *P.*
509 *aeruginosa* PDO300, PDO300 (*Δpel*) and PDO300(*Δpsl*) mutant strains were gratefully received
510 from Professor Bernd H. A. Rehm, Institute of Molecular Biosciences, Massey University, New
511 Zealand (28), where PDO300 is an isogenic *mucA* deletion mutant of PAO1 that overproduces
512 alginate. PDO300, PDO300 (*Δpel*), PDO300(*Δpsl*) and PAO1 (*Δpf4),* were also grown in LB at
513 37°C. *P. protogens Pf-5* and *P. putida* ATCC BAA-477 and S12 strain were grown in LB at
514 30°C.

515 Biofilm growth assay

516 Ten milliliter aliquots of *P. aeruginosa* planktonic pre-cultures (LB, 200 rpm, 37°C, OD_{600} 2.40,
517 16 h) were diluted 50 times with LB in 2 L Erlenmeyer flasks and incubated for 5 d under static
518 conditions. Supplementary Figure 14A displays an image of 5 d old biofilm in LB. The cultures
519 were centrifuged at 10,000 x *g* for 15 min, the supernatant removed by decanting, and the

520 biofilm then collected and lyophilized (LabConco). Supplementary Figure 14B displays an
521 image of the culture after centrifugation showing clear separation of biofilm and supernatant.

522 **Enzymatic digestions**

523 Twenty milligrams of lyophilized biofilm was resuspended in 1 mL of either i) RNase buffer (50
524 mM Tris HCl, 10 mM EDTA, pH8) with 0.2 mg RNaseA from bovine pancreas (Sigma Aldrich),
525 ii) storage buffer (10 mM NaCl, 10 mM Tris-HCl) with 0.1 mg Pronase E from *Streptomyces*
526 *grisens* (Sigma Aldrich) with 0.5% (v/v), iii) 1X RNase H reaction buffer (20 mM Tris-HCl pH
527 7.8, 40 mM KCl, 8 mM $MgCl_2$, 1 mM DTT) with 0.4 mg RNase H (Thermo Fisher Scientific),
528 iv) 1X RNase III reaction buffer (500 mM NaCl, 100 mM Tris pH 7.9, 100 mM $MgCl_2$, 10 mM
529 DTT) with 0.6 mg RNase II (Thermo Fisher Scientific) or v) DNase I buffer (100 mM Tris (pH
530 7.5), 25 mM $MgCl_2$ and $CaCl_2$) with 0.2 mg DNAse I (active and inactivated) from bovine
531 pancreas (Sigma Aldrich). DNase I was inactivated with the addition of 1 mM EDTA and
532 following heating to 85°C in DNase I buffer for 10 min. All digestions were performed with
533 shaking at 200 rpm at 37°C for 16 h. The suspensions were then centrifuged (10,000 x *g*, 15
534 min), the supernatant was discarded and the pellets of the biofilm materials were lyophilized.

535 **Normal force measurement**

536 Forty milligrams per milliliter solutions of lyophilized biofilms were added to 1 mL 1-ethyl-3-
537 methylimidazolium acetate and incubated at 55°C for 2 h. A Haake Mars 3 (Thermo Fisher
538 Scientific) stress-controlled rotational rheometer with Peltier controlled element at 25°C, was
539 used for rheological measurements. Thirty five-millimeter diameter parallel plate geometry was
540 used with smooth titanium plates to measure viscosity and normal stress difference ($N_1 - N_2$)
541 where N_1 is the difference between normal stresses in the direction of shearing and those oriented
542 perpendicular to the shear plane, and N_2 the difference between normal stresses perpendicular to

543 the shear plane and those in the neutral, traverse, direction (26). Prior to measurement, the gap
544 error was zeroed at 4 N and gap error calculated as previously described (60-62). The parallel
545 plate rheometer was used because it allows rheological characterization of ultra-low sample
546 volumes and permits access to high shear rates for characterization of non-linear elasticity
547 without measurement artifacts such as inertia (i.e. Reynolds number is low). One hundred
548 microliters of sample were deposited on the plates. The plates were closed to 100 μm, the sample
549 trimmed and the sample allowed to sit for 5 min prior to measurement. All measurements with
550 Normal force (F_N) less than the resolution of the rheometer (i.e. < 0.1 N) were set to 0 before
551 calculation of N_1-N_2 using equations 9-11, and viscosity from equation 3-5 in Davies and Stokes
552 (60) for the parallel plate geometry.

553 Only the linearly increasing portion of the normal stress difference curves are presented. Above
554 this range normal stress difference begins to decrease again which may be due to elastic
555 instabilities or associating polymers (63). Corrections were made to $N_1 - N_2$ to account for inertia
556 using equation 17 in Davies and Stokes (60) and to correct for the baseline residual force in the
557 samples. Except for the DNase I-treated biofilm, the shear rheology for all treatments could be
558 modelled using the finitely extensible non-linear elastic with Gaussian closure proposed by
559 Peterlin (FENE-P) constitutive model by varying four parameters to fit shear viscosity and
560 normal stress difference as a function of shear rate (Supplementary Table 2). To use this model,
561 we make the assumption that $N_2 << N_1$, and thus $\Delta N \sim N_1$, as is common for polymer solutions
562 (Davies and Stokes (60)). Fitting parameters for the FENE-P model include λ_1 = relaxation
563 time, b = a measure of the relative extensibility of the model spring, η_s = solvent viscosity, η_p =
564 polymer contribution to the viscosity. The FENE-P equations can be written in the following
565 format, as shown by Bird et al.(61):

566 $$\eta = \eta_s + \frac{\eta_p}{\lambda_1 \dot{\gamma}}\left((C_2 + C_1)^{\frac{1}{3}} - (C_2 - C_1)^{\frac{1}{3}}\right) \quad \text{(Equation 1)}$$

567

568 $$N_1 = \frac{2\eta_p}{\lambda_1}\left((C_2 + C_1)^{\frac{1}{3}} - (C_2 - C_1)^{\frac{1}{3}}\right)^2 \quad \text{(Equation 2)}$$

569 Where:

570 $$C_1 = \frac{b}{4}\lambda_1 \dot{\gamma} \quad \text{(Equation 3)}$$

571 $$C_2 = \left(C_1^2 + \left(\frac{b+3}{6}\right)^3\right)^{1/2} \quad \text{(Equation 4)}$$

572

573 All measurements were performed in triplicate. For clarity, one representative data set is
574 presented in Figure 1A-B and Supplementary Figure 1A-B, with the respective Power Law and
575 FENE-P model fit to that data set. Averaged values for the FENE-P and Power law fits, with the
576 standard deviation across three biological replicates are shown in Supplementary Tables 1 and 2,
577 where each biological replicate refers to a separate growth assay.

578 For oscillatory measurements a Haake Mars 60 (Thermo Scientific) stress-controlled rotational
579 rheometer with Peltier controlled element at 25°C was used. 0.25 mL biofilm (native wild type,
580 wild type following digestion with active and inactivated DNase I, RNase III and RNase H,
581 PDO300(*Δpel*) and PDO300(*Δpsl*) and eDNA gel were collected from solution and deposited on
582 thirty five-millimeter diameter parallel plate geometry with smooth titanium plates, which were
583 closed to 250 µm, and the sample trimmed prior to measurement. A frequency range of 0.1 to 1
584 s^{-1} was used and at a strain in the linear viscoelastic region for each of the samples analyzed.

585 **Extracellular polymeric substances (EPS) extraction**

586 Lyophilized biofilms were dissolved in ionic liquid mixture (40% (v/v) 1-ethyl-3-
587 methylimidazolium acetate (EMIM Ac): 60% (v/v) N,N-dimethyl acetamide (DMAc)) at 55°C
588 for 16 h. The solution was centrifuged (10,000 x *g*) to remove any undissolved material.
589 Perchloric acid (70%) was added (0.05% v/v) to the viscosified centrate (on ice). After 15 min
590 incubation, the solution was centrifuged at 10,000 x *g* at 4°C for 15 min and the pellet recovered.
591 This was repeated on the centrate two to four times until the solution was not viscous. The
592 precipitate was dialysed against double distilled water for 2 d at 4°C (SnakeSkin™ Dialysis
593 Tubing, 3.5K MWCO, 22 mm) and the retentate lyophilized (FreeZone Plus 4.5 Liter Cascade
594 Benchtop Freeze Dry System). The same procedure was performed in triplicate on calf thymus
595 DNA, lipase, cytochrome C for the purposes of determining recovery yield of representative
596 exoproteins, and on RNA from torula yeast for assessing by ^{31}P NMR whether the extraction
597 procedure contributed to RNA transesterification (all from Sigma Aldrich).

598 **Extracellular nucleic acid isolation**

599 Twenty milligrams of lyophilized retentate (i.e. post perchloric acid precipitation) were dissolved
600 in 1 mL of 40% (v/v) EMIM-Ac, 60% DMAc (v/v) (55°C, 16 h). Chromatographic separation
601 was achieved in a Shimadzu system comprising DGU-20A 3r Prominence Degasser and LC-
602 20AD Solvent Delivery Unit, fitted with two Agilent PLgel 10 µm column of 10^5Å pore size for
603 separation across the MW range 200 kDa to 2000 kDa. The eluent flow rate was 3.0 mL.min^{-1}
604 and the injection volume 1 mL. The fractions with molecular weight range of 2000-800kDa and
605 800-200kDa were pooled, precipitated with 60% v/v ethanol, and the precipitate resuspended in
606 doubled distilled water and dialyzed for 2 d at 4°C (SnakeSkin™ Dialysis Tubing, 3.5K MWCO,
607 22 mm) against double distilled water to induce gelation. The gel was then collected from the
608 dialysis tubing.

609 **eDNA temperature-dependent phase transition**

610 Five-day old biofilm and eDNA gel isolate were resuspended in double distilled water to achieve
611 UV absorbance reading 1 and ddH_2O served as a blank. The heat-treated samples were analyzed
612 by JASCO-815 spectropolarimeter in a 1 cm path length quartz cuvette containing a solution
613 volume 500 µL. Spectra (200-320 nm) were measured at 1°C increments from 30 - 95°C. For
614 each measurement, an average of three scans was taken and the buffer spectra subtracted. The
615 magnitude of the DNA peak presented is the rolling average across five temperatures. The
616 differential scanning calorimetry thermogram was measured in a MicroSC multicell calorimeter
617 (Setaram,), using Calisto for data collection and processing. 400 and 60 mg of 5 d biofilm and
618 eDNA gel isolates respectively added to sealed-1 mL Hastelloy C cells for measurement. An
619 empty HastelloyC cell was used as reference. The samples were heated from 20-100°C at 1
620 $K.min^{-1}$, then cooled down to 20°C at 1 $K.min^{-1}$. The experiment was run under nitrogen gas
621 sweeping.

622 **Solid-state NMR**

623 For solid-state NMR experiments performed on the eDNA gel isolate, ^{15}N labeled NH_4Cl-
624 supplemented M9 minimal media was used for biofilm growth. M9 consisted of 9.552 $g.L^{-1}$
625 $Na_2HPO_4.2H_2O$, 4.41 g $litre^{-1}$ KH_2PO_4, 1.71 $g.L^{-1}$ NaCl, 1 $g.L^{-1}$ $^{15}NH_4Cl$, 0.24 $g.L^{-1}$ $MgSO_4$,
626 0.011 $g.L^{-1}$ $CaCl_2$, 2 $g.L^{-1}$ casamino acids, and 0.4 $g.L^{-1}$ glucose. The eDNA gel was prepared
627 from the M9 grown *P. aeruginosa* PAO1 biofilm as described above.

628 Solid-state NMR experiments were performed on 1) eDNA gel with and 2) without preheating to
629 65°C, and 3) chromosomal DNA after lyophilization, dissolution in (EMIM Ac): 60% (v/v)
630 N,N-dimethyl acetamide (DMAc)) at 55°C for 16 h, precipitation with ethanol (60% v/v) and
631 dialysis against water (3500 Da MWCO) as described above for eDNA. A 14.1 T Bruker

632 Advance III instruments was used equipped with a 1.9 mm MAS probe operated in double mode.
633 The typical ^{1}H, ^{15}N and ^{31}P $\pi/2$ pulse lengths were 2.3, 3.7, and 4.5 μs, respectively. 2D dipolar-
634 based ^{15}N-^{1}H heteronuclear-correlation (HETCOR) experiments were conducted on the ^{15}N-
635 labelled eDNA gel isolate at 37 kHz MAS spinning frequency. Variable temperature was
636 regulated at -20ºC and the sample temperature was 12ºC (calibrated using ethylene glycol). In
637 the ^{15}N-^{1}H HETCOR experiments, the initially excited ^{1}H magnetization was transferred to ^{15}N
638 through a cross polarization step followed by t1 evolution. Then, the ^{15}N magnetization was
639 flipped to longitudinal axis and 400 ms proton saturation pulses were applied for water
640 suppression. Subsequently, the ^{15}N magnetization was flipped to the transverse plane and
641 transferred to ^{1}H via a second CP step for signal acquisition. Two ^{15}N-^{1}H HETCOR experiments
642 were collected, one with 400 μs and the other with 2 ms contact times applied for both of the CP
643 steps. Low power XiX ^{1}H decoupling (~10 kHz) was employed during ^{15}N evolution and
644 WALTZ-16 decoupling (10 kHz) was implemented on ^{15}N channel during ^{1}H acquisition.
645 1-D ^{31}P experiments were performed on ^{15}N-labelled eDNA gel isolate and ^{15}N-labelled *P.*
646 *aeruginosa* PAO biofilm, both directly after dialysis against double distilled water at 4°C for 2 d
647 (SnakeSkin™ Dialysis Tubing, 3.5K MWCO, 22 mm) and following alkalinization (0.1 M
648 NaOD, 55ºC, 15 min) and lyophilization (FreeZone Plus 4.5 Liter Cascade Benchtop Freeze Dry
649 System). 15 kHz MAS spinning frequency and a sample temperature of 27ºC. 75 kHz
650 SPINAL64 ^{1}H decoupling was applied during ^{31}P acquisition time. All chemical shifts were
651 indirectly referenced using adamantane as a secondary standard (downfield peak is at 40.48 ppm,
652 DSS scale).

653 **Solution-state nuclear magnetic resonance (NMR)**

654 Solution-state NMR experiments were performed on an 800 MHz Bruker Avance III
655 spectrometer at 25°C. Sample concentration was 10 mg (dry weight).mL^{-1} unless otherwise
656 specified. Spectra were recorded either under conditions of neutral pH in 100% D_2O (Cambridge
657 Isotope Laboratories), or following alkalinization (i.e. transesterification, 0.1 M NaOD, 55°C, 2
658 h). 1-D NMR experiments include ^{1}H and ^{31}P direct detection, while 2-D NMR analysis include
659 ^{13}C-HSQC, ^{13}C-HSQC-TOCSY, ^{1}H-^{31}P HETCOR, HMBC, and COSY. All spectra were
660 referenced internally against the solvent peak (90% H2O and 10% D2O, unless otherwise
661 specified), and all spectral analyses were performed using Topspin 4.0 and NMRFAM-SPARKY
662 (64) software.
663 Asolectin (Sigma Aldrich) standard (10 mg/mL) and lyophilized *P. aeruginosa* PAO1 biofilm (10
664 mg/mL) were dissolved in 40% (v/v) EMIM Ac: 60% (v/v) DMAc at (55°C, 2 h). *P. aeruginosa*
665 PAO1 pre-culture cell lysate was prepared by lysing pre-culture cells with lysozyme in PBS. 10%
666 (v/v) of D_2O was added to all samples for locking purposes.

667 **Chromosomal DNA extraction**

668 Chromosomal DNA was extracted from the biofilm using FastDNA SPIN Kit for soil (MP
669 Biomedicals, USA) as per the standard protocol. Briefly, biofilm was resuspended in Sodium
670 Phosphate Buffer in was lysed (Lysing Matrix), homogenized (FastPrep®, 40 seconds, speed
671 setting 6.0), and the cell debris removed by centrifugation (14,000 x *g*, 5 min). Proteins were
672 removed by precipitation (250 µl Protein Precipitation Solution), the supernatant mixed with
673 DNA Binding Matrix, which was then homogenized and transferred to a SPIN™ Filter. Excess
674 supernatant was removed by centrifugation (14,000 x *g*, 5 min). DNA was then eluted from air
675 dried DNA Binding Matrix with DNase/ Pyrogen-Free Water.

676 **Nucleotide sequencing, size and compositional analysis**

677 The eDNA gel isolate was resuspended in 500 uL of 1x Protease K solution (10× Protease K
678 solution: 10 mM Tris HCl, 1% SDS and 10 mM EDTA, pH 8 buffer (10× protease K buffer
679 containing 500 mM Tris-HCl, 10% SDS, 10 mM $CaCl_2$) and 10 µL of Protease K (20 $mg.mL^{-1}$,
680 Thermo Fisher Scientific) was added and the mixture incubated at 60°C for 2-16 h, after which
681 DNA was extracted as previously described in the phenol-chloroform method (65).
682 Samples before sequencing were further purified to remove any remaining protein and RNA by
683 RNase and Proteinase K treatment. The DNA was then isolated using phenol-chloroform
684 precipitation as described above. The DNA precipitate was dissolved in TE buffer, the purity
685 confirmed by 260/280 value in Nanodrop (acceptable range value: 1.8-2.0) and Qubit® 2.0
686 fluorometer.

687 The molecular weight distributions of extracellular and genomic DNA were measured on a 1%
688 agarose gel, which was prepared from Viviantis LE grade agarose using 1x TAE buffer (40 mM
689 Tris, 20 mM Acetate and 1 mM EDTA, pH 8.6). Gels were run horizontally. After
690 electrophoresis, the gel was stained for 0.5 h with ethidium bromide and visualized under
691 UV(66).
692 Three biological replicates were used for each DNA sequence analysis. Library was produced
693 using Illumina DNA sample preparation kit. The libraries were sequenced using Illumina MiSeq
694 platform (Illumina, San Diego, Ca) with paired-end protocol to read lengths of 600 nt generating
695 a total of 1,614,106 and 1,848,846 paired end reads. Raw reads were quality filtered (reads
696 remaining after trimming: PPG1-1549104, PBLC1-1666280) and aligned to the *P. aeruginosa*
697 PAO1 (AE004091) genome using CLC Genomics Workbench 9.0 (CLC bio, Cambridge, MA).
698 Extracellular RNA length was determined by TapeStation, model 2200 (Agilent Technologies).

699 Monoribonucleotide quantification was achieved on three biological replicates of the nucleic
700 acid isolate gels, pre-alkalinized with 0.4 M NaOH in double distilled water (10 mg dry weight
701 gel/mL) at 55 °C for 2 h. Extracellular monoribonucleotides resulting from transesterification
702 were quantified using Waters ACQUITY UPLC™ (Waters Milford, MA) liquid chromatography
703 system with XEVO TQ-S mass spectrometer (Waters Milford, MA) equipped with an
704 electrospray ionization (ESI) source. 2 µl of diluted samples were injected for analysis. An
705 AQUITY UPLC HSS T3 column (2.1 mm x 150 mm, 1.7 µm, Waters, USA) was used,
706 maintained at 45°C. 0.1% v/v formic acid and acetonitrile were used to establish the required
707 gradient. The elution gradient increased from 0-1% v/v acetonitrile in first 6 min and then to
708 100% at 7 min, which was maintained for another 1.5 min, reduced to 0% at 8.6 min and held
709 until 12 min. Torula yeast RNA (0.5 mg/L) was used as RNA standard (Sigma Aldrich). The
710 HPLC flow rate was maintained at 0.3 $ml.min^{-1}$.

711 **Staining and microscopy**

712 Microscopic imaging was conducted on a confocal microscope Zeiss LSM 780 with a 63×
713 objective. Extracellular RNA in the gel isolate were stained using SYTO RNASelect (Thermo
714 Fisher Scientific) green fluorescent cell stain (5 mM solution in DMSO). Five µM stain solution
715 was prepared from 1 µL of stock in 1X PBS solution (137 mM NaCl**,** 2.7 mM KCl**,** 4.3 mM
716 Na_2HPO_4**,** 1.47 mM KH_2PO_4). The gel isolate was labelled with 5 µM stain solution, kept at
717 37°C for 20 min and then transferred to glass side for imaging. eDNA staining was achieved by
718 depositing biofilm or eDNA gel isolate on a glass slide, air-drying overnight and incubating with
719 2 µM TOTO-1 iodide (1 mM solution in DMSO, Thermo Fisher Scientific) for 15 min.

720

Acknowledgments

We acknowledge Prof Bernd Rehm for supplying polysaccharide deletion mutants of *P. aeruginosa*, Dan Roizman for providing *P. putida,* Long Yu for assistance with rheology, Dr Gleb Yakubov for coordinating sample preparation for rheological measurements, Ravi Jagadeeshan for discussion regarding DNA normal force analysis, and Florentin Constancias for analyzing the sequencing data. SCELSE is funded by Singapore's Ministry of Education, National Research Foundation, Nanyang Technological University (NTU), and National University of Singapore (NUS) and hosted by NTU in partnership with NUS. J.R.S acknowledges the assistance of Australian Research Council Discovery Project DP180101919.

Author Contributions

T.S., F.R.W., W.L.L., S.M., H.M.S., S.S.A. and X.S. performed experiments; T.S. and A.T.P. designed the experiments. T.S. (all), F.R.W. (nucleic acids), A.T.P. (nucleic acids), H.M.S. (rheology), G.S.K. (sequencing), S.S.A. (LCMS/MS) and J.R.S. (rheology) advised on measurements and analysed the data. T.S., F.R.W., W.L.L., H.M.S., S.A.R., A.T.P and S.K. wrote the manuscript. J.R.S edited the manuscript.

Competing Interests

All authors have no competing interests.

References

1. Phillips, P.L. and Schultz, G.S. (2012) Molecular mechanisms of biofilm infection: biofilm virulence factors. *Adv. Wound Care*, **1**, 109-114.
2. Drescher, K., Shen, Y., Bassler, B.L. and Stone, H.A. (2013) Biofilm streamers cause catastrophic disruption of flow with consequences for environmental and medical systems. *Proc. Natl. Acad. Sci. U. S. A*. **110**, 4345-4350.

745 3. Seviour, T., Lambert, L.K., Pijuan, M. and Yuan, Z. (2011) Selectively inducing the
746 synthesis of a key structural exopolysaccharide in aerobic granules by enriching for
747 *Candidatus* 'Competibacter phosphatis'. *Appl. Microbiol. Biotechnol*, **92**, 1297-1305.
748 4. Høiby, N., Bjarnsholt, T., Givskov, M., Molin, S.R. and Ciofu, O. (2010) Antibiotic
749 resistance of bacterial biofilms. *Int. J. Antimicrob. Agents*, **35**, 322-332.
750 5. Kurniawan, A., Yamamoto, T., Tsuchiya, Y. and Morisaki, H. (2012) Analysis of the ion
751 adsorption–desorption characteristics of biofilm matrices. *Microbes Environ*, **27**, 399-
752 406.
753 6. de Kreuk, M.K., Picioreanu, C., Hosseini, M., Xavier, J.B. and van Loosdrecht, M.C.M.
754 (2007) Kinetic model of a granular sludge SBR: Influences on nutrient removal.
755 *Biotechnol. Bioeng*, **97**, 801-815.
756 7. Flemming, H.-C. and Wingender, J. (2010) The biofilm matrix. *Nat. Rev. Microbiol*, **8**,
757 623-633.
758 8. Gloag, E.S., Fabbri, S., Wozniak, D.J. and Stoodley, P. (2020) Biofilm mechanics:
759 Implications in infection and survival. *Biofilm*, **2**, 100017.
760 9. Bodey, G.P., Bolivar, R., Fainstein, V. and Jadeja, L. (1983) Infections caused by
761 *Pseudomonas aeruginosa*. *Rev. Infect. Dis*, **5**, 279-313.
762 10. Colvin, K.M., Irie, Y., Tart, C.S., Urbano, R., Whitney, J.C., Ryder, C., Howell, P.L.,
763 Wozniak, D.J. and Parsek, M.R. (2012) The Pel and Psl polysaccharides provide
764 *Pseudomonas aeruginosa* structural redundancy within the biofilm matrix. *Environ.*
765 *Microbiol*, **14**, 1913-1928.
766 11. Seviour, T., Hansen, S.H., Yang, L., Yau, Y.H., Wang, V.B., Stenvang, M.R.,
767 Christiansen, G., Marsili, E., Givskov, M., Chen, Y. *et al.* (2015) Functional amyloids
768 keep quorum-sensing molecules in check. *J. Biol. Chem*, **290**, 6457-6469.
769 12. Borlee, B.R., Goldman, A.D., Murakami, K., Samudrala, R., Wozniak, D.J. and Parsek,
770 M.R. (2010) *Pseudomonas aeruginosa* uses a cyclic-di-GMP-regulated adhesin to
771 reinforce the biofilm extracellular matrix. *Mol. Microbiol*, **75**, 827-842.
772 13. Allesen-Holm, M., Barken, K.B., Yang, L., Klausen, M., Webb, J.S., Kjelleberg, S.,
773 Molin, S., Givskov, M. and Tolker-Nielsen, T. (2006) A characterization of DNA release
774 in *Pseudomonas aeruginosa* cultures and biofilms. *Mol. Microbiol*, **59**, 1114-1128.
775 14. Okshevsky, M. and Meyer, R.L. (2015) The role of extracellular DNA in the
776 establishment, maintenance and perpetuation of bacterial biofilms. *Crit. Rev. Anal. Chem*,
777 **41**, 341-352.
778 15. Whitchurch, C.B., Tolker-Nielsen, T., Ragas, P.C. and Mattick, J.S. (2002) Extracellular
779 DNA required for bacterial biofilm formation. *Science*, **295**, 1487.
780 16. Böckelmann, U., Janke, A., Kuhn, R., Neu, T.R., Wecke, J., Lawrence, J.R. and
781 Szewzyk, U. (2006) Bacterial extracellular DNA forming a defined network-like
782 structure. *FEMS Microbiol. Lett*, **262**, 31-38.
783 17. Jennings, L.K., Storek, K.M., Ledvina, H.E., Coulon, C., Marmont, L.S., Sadovskaya, I.,
784 Secor, P.R., Tseng, B.S., Scian, M., Filloux, A. *et al.* (2015) Pel is a cationic
785 exopolysaccharide that cross-links extracellular DNA in the *Pseudomonas aeruginosa*
786 biofilm matrix. *Proc. Natl. Acad. Sci. U. S. A* , **112**, 11353-11358.
787 18. Cherny, K.E. and Sauer, K. (2019) *Pseudomonas aeruginosa* Requires the DNA-Specific
788 Endonuclease EndA To Degrade Extracellular Genomic DNA To Disperse from the
789 Biofilm. *J. Bacteriol,* **201**, e00059-00019

19. Turnbull, L., Toyofuku, M., Hynen, A.L., Kurosawa, M., Pessi, G., Petty, N.K., Osvath, S.R., Carcamo-Oyarce, G., Gloag, E.S., Shimoni, R. *et al.* (2016) Explosive cell lysis as a mechanism for the biogenesis of bacterial membrane vesicles and biofilms.*Nat.Commun*, **7**, 11220.
20. Niki, H., Yamaichi, Y. and Hiraga, S. (2000) Dynamic organization of chromosomal DNA in *Escherichia coli*. *Genes Dev*, **14**, 212-223.
21. Devaraj, A., Justice, S.S., Bakaletz, L.O. and Goodman, S.D. (2015) DNABII proteins play a central role in UPEC biofilm structure. *Mol. Microbiol*, **96**, 1119-1135.
22. Zhao, H. (2015) DNA stability in ionic liquids and deep eutectic solvents. *J. Chem. Technol. Biotechnol*, **90**, 19-25.
23. Vitz, J., Erdmenger, T., Haensch, C. and Schubert, U.S. (2009) Extended dissolution studies of cellulose in imidazolium based ionic liquids. *Green Chem*, **11**, 417-424.
24. Seviour, T., Weerachanchai, P., Hinks, J., Roizman, D., Rice, S.A., Bai, L., Lee, J.-M. and Kjelleberg, S. (2015) Solvent optimization for bacterial extracellular matrices: a solution for the insoluble. *RSC Adv*, **5**, 7469-7478.
25. Scirocco, R., Vermant, J. and Mewis, J. (2005) Shear thickening in filled Boger fluids. *J. Rheol (N.Y.)* **49**, 551-567.
26. Verrelli, D.I. and Kilcullen, A.R. (2016) Normal Stress Differences and Yield Stresses in Attractive Particle Networks. *Adv. Cond. Matter. Phys*, **2016**, 21.
27. Stokes, J.R., Graham, L.J.W., Lawson, N.J. and Boger, D.V. (2001) Swirling flow of viscoelastic fluids. Part 2. Elastic effects. *J. Fluid Mech*, **429**, 117-153.
28. Ghafoor, A., Hay, I.D. and Rehm, B.H.A. (2011) Role of exopolysaccharides in *Pseudomonas aeruginosa* biofilm formation and architecture. *Appl. Environ. Microbiol*, **77**, 5238-5246.
29. Mansfield, M.L., Tsortos, A. and Douglas, J.F. (2015) Persistent draining crossover in DNA and other semi-flexible polymers: Evidence from hydrodynamic models and extensive measurements on DNA solutions. *J. Chem. Phys*, **143**, 124903.
30. Elkin, I., Weight, A.K. and Klibanov, A.M. (2015) Markedly lowering the viscosity of aqueous solutions of DNA by additives. *Int. J. Pharm*, **494**, 66-72.
31. Kypr, J., Kejnovská, I., Renčiuk, D. and Vorlíčková, M. (2009) Circular dichroism and conformational polymorphism of DNA. *Nucleic Acids Res*, **37**, 1713-1725.
32. Greenfield, N.J. (2006) Using circular dichroism spectra to estimate protein secondary structure. *Nat. Protoc*, **1**, 2876-2890.
33. del Villar-Guerra, R., Trent, J.O. and Chaires, J.B. (2018) G-Quadruplex secondary structure obtained from circular dichroism spectroscopy. *Angew. Chem., Int. Ed*, **57**, 7171-7175.
34. Reichhardt, C. and Cegelski, L. (2014) Solid-state NMR for bacterial biofilms. *Mol. Phys*, **112**, 887-894.
35. Marchanka, A., Simon, B., Althoff-Ospelt, G. and Carlomagno, T. (2015) RNA structure determination by solid-state NMR spectroscopy. *Nat. Commun* , **6**, 7024.
36. Feigon, J., Koshlap, K.M. and Smith, F.W. (1995) *[10]1H NMR spectroscopy of DNA triplexes and quadruplexes*. *Academic Press*.
37. Hänsel-Hertsch, R., Di Antonio, M. and Balasubramanian, S. (2017) DNA G-quadruplexes in the human genome: detection, functions and therapeutic potential. *Nat. Rev. Mol. Cell Biol*, **18**, 279.

835 38. Friedman, L. and Kolter, R. (2004) Two genetic loci produce distinct carbohydrate-rich
836 structural components of the *Pseudomonas aeruginosa* biofilm matrix.
837 *J. Bacteriol*, **186**, 4457-4465
838 39. Wüthrich, K. (2008) *NMR of proteins and nucleic acids*. 2 ed. John Wiley and Sons, New
839 York.
840 40. Shen, K., Sayeed, S., Antalis, P., Gladitz, J., Ahmed, A., Dice, B., Janto, B., Dopico, R.,
841 Keefe, R., Hayes, J. *et al.* (2006) Extensive genomic plasticity in *Pseudomonas*
842 *aeruginosa* revealed by identification and distribution studies of novel genes among
843 clinical isolates. *Infect. Immun*, **74**, 5272-5283.
844 41. Radak, B.K., Harris, M.E. and York, D.M. (2013) Molecular simulations of RNA 2′-o-
845 transesterification reaction models in solution. *J. Phys. Chem. B*, **117**, 94-103.
846 42. Okshevsky, M. and Meyer, R.L. (2014) Evaluation of fluorescent stains for visualizing
847 extracellular DNA in biofilms. *J. Microbiol. Methods*, **105**, 102-104.
848 43. Cornwell, D.J. and Smith, D.K. (2015) Expanding the scope of gels - Combining
849 polymers with low-molecular-weight gelators to yield modified self-assembling smart
850 materials with high-tech applications. *Mater. Horiz*, **2**, 279-293.
851 44. Chen, Y.Z., Bennett, C.L., Huynh, H.M., Blair, I.P., Puls, I., Irobi, J., Dierick, I., Abel,
852 A., Kennerson, M.L., Rabin, B.A. *et al.* (2004) DNA/RNA helicase gene mutations in a
853 form of juvenile amyotrophic lateral sclerosis (ALS4). *Am. J. Hum. Genet*, **74**, 1128-
854 1135.
855 45. Nakamura, H., Oda, Y., Iwai, S., Inoue, H., Ohtsuka, E., Kanaya, S., Kimura, S.,
856 Katsuda, C., Katayanagi, K. and Morikawa, K. (1991) How does RNase H recognize a
857 DNA.RNA hybrid? *Proc. Natl. Acad. Sci. U. S. A* , **88**, 11535-11539.
858 46. Geerts-Dimitriadou, C., Lu, Y.-Y., Geertsema, C., Goldbach, R. and Kormelink, R.
859 (2012) Analysis of the Tomato spotted wilt virus Ambisense S RNA-Encoded Hairpin
860 Structure in Translation. *PloS one*, **7**, e31013.
861 47. Singh, N., Sharma, M., Mondal, D., Pereira, M.M. and Prasad, K. (2017) Very high
862 concentration solubility and long-term stability of DNA in an ammonium-based ionic
863 liquid: a suitable medium for nucleic acid packaging and preservation.
864 ***ACS*** *Sustain.* ***Chem****. Eng*, **5**, 1998-2005.
865 48. Seviour, T., Pijuan, M., Nicholson, T., Keller, J. and Yuan, Z. (2009) Gel-forming
866 exopolysaccharides explain basic differences between structures of aerobic sludge
867 granules and floccular sludges. *Water Res*, **43**, 4469-4478.
868 49. Xing, Y., Cheng, E., Yang, Y., Chen, P., Zhang, T., Sun, Y., Yang, Z. and Liu, D.
869 (2011) Self-Assembled DNA Hydrogels with Designable Thermal and Enzymatic
870 Responsiveness. *Adv. Mater*, **23**, 1117-1121.
871 50. Jain, A. and Vale, R.D. (2017) RNA phase transitions in repeat expansion disorders.
872 *Nature*, **546**, 243-247.
873 51. Raychaudhuri, A. and Tipton, P.A. (2004) Protocol for amplification of GC-rich
874 sequences from *Pseudomonas aeruginosa*. *BioTechniques*, **37**, 752-756.
875 52. Collins, L.J., Schönfeld, B. and Chen, X.S. (2011) In Tollefsbol, T. (ed.), *Handbook of*
876 *Epigenetics*. Academic Press, San Diego, pp. 49-61.
877 53. Nadel, J., Athanasiadou, R., Lemetre, C., Wijetunga, N.A., Ó Broin, P., Sato, H., Zhang,
878 Z., Jeddeloh, J., Montagna, C., Golden, A. *et al.* (2015) RNA:DNA hybrids in the human
879 genome have distinctive nucleotide characteristics, chromatin composition, and
880 transcriptional relationships. *Epigenet. chromatin*, **8**, 46.

881 54. Flemming, H.-C., Wingender, J., Szewzyk, U., Steinberg, P., Rice, S.A. and Kjelleberg,
882 S. (2016) Biofilms: an emergent form of bacterial life. *Nat. Rev. Microbiol*, **14**, 563.
883 55. Mann, E.E., Rice, K.C., Boles, B.R., Endres, J.L., Ranjit, D., Chandramohan, L., Tsang,
884 L.H., Smeltzer, M.S., Horswill, A.R. and Bayles, K.W. (2009) Modulation of eDNA
885 release and degradation affects *Staphylococcus aureus* biofilm maturation. *PLoS One*, **4**,
886 e5822.
887 56. Adam, B., Baillie, G.S. and Douglas, L.J. (2002) Mixed species biofilms of *Candida*
888 *albicans* and *Staphylococcus epidermidis*. *J. Med. Microbiol*, **51**, 344-349.
889 57. Rose, S.J., Babrak, L.M. and Bermudez, L.E. (2015) *Mycobacterium avium* possesses
890 extracellular DNA that contributes to biofilm formation, structural integrity, and
891 tolerance to antibiotics. *PLOS ONE*, **10**, e0128772.
892 58. Cheng, M., Cook, A.E., Fukushima, T. and Bond, P.L. (2011) Evidence of compositional
893 differences between the extracellular and intracellular DNA of a granular sludge biofilm.
894 *Lett. appl. microbiol*, **53**, 1-7.
895 59. Rice, S.A., Tan, C.H., Mikkelsen, P.J., Kung, V., Woo, J., Tay, M., Hauser, A.,
896 McDougald, D., Webb, J.S. and Kjelleberg, S. (2009) The biofilm life cycle and
897 virulence of *Pseudomonas aeruginosa* are dependent on a filamentous prophage. *The*
898 *ISME journal*, **3**, 271-282.
899 60. Davies, G.A. and Stokes, J.R. (2008) Thin film and high shear rheology of multiphase
900 complex fluids. *J. Non-Newton. fluid* , **148**, 73-87.
901 61. Bird, R.B., Armstrong, R.C. and Hassager, O. (1987) *Dynamics of polymeric liquids. Vol.*
902 *1, 2nd Ed.: Fluid mechanics*. John Wiley and Sons Inc.,New York, NY, United States.
903 62. Kravchuk, O. and Stokes, J.R. (2013) Review of algorithms for estimating the gap error
904 correction in narrow gap parallel plate rheology. *J. Rheol*, **57**, 365-375.
905 63. Annable, T., Buscall, R., Ettelaie, R. and Whittlestone, D. (1993) The rheology of
906 solutions of associating polymers: Comparison of experimental behavior with transient
907 network theory. *J. Rheol*, **37**, 695-726.
908 64. Lee, W., Tonelli, M. and Markley, J.L. (2014) NMRFAM-SPARKY: enhanced software
909 for biomolecular NMR spectroscopy. *Bioinformatics*, **31**, 1325-1327.
910 65. Ausubel, F.M. (2002) *Short protocols in molecular biology : a compendium of methods*
911 *from Current protocols in molecular biology*. 5th ed. Wiley, New York.
912 66. Lee, P.Y., Costumbrado, J., Hsu, C.-Y. and Kim, Y.H. (2012) Agarose gel
913 electrophoresis for the separation of DNA fragments. *J. Vis. exp: JoVE*, 3923.
914